Poissonian Cellular Potts Models Reveal Nonequilibrium Kinetics of Cell Sorting

(Article begins on next page)

22 December 2024

Poissonian Cellular Potts Models Reveal Nonequilibrium Kinetics of Cell Sorting

R. Belousov[1,*] S. Savino[1,2] P. Moghe[3,4] T. Hiiragi[3,5,6] L. Rondoni[2,7] and A. Erzberger[1,8,†]

[1]*Cell Biology and Biophysics Unit, European Molecular Biology Laboratory, Meyerhofstraße 1, 69117 Heidelberg, Germany*
[2]*Department of Mathematical Sciences, Politecnico di Torino, Corso Duca degli Abruzzi 24, 10129 Turin, Italy*
[3]*Hubrecht Institute, Uppsalalaan 8, 3584 CT Utrecht, Netherlands*
[4]*Developmental Biology Unit, European Molecular Biology Laboratory, Meyerhofstraße 1, 69117 Heidelberg, Germany*
[5]*Institute for the Advanced Study of Human Biology (WPI-ASHBi), Kyoto University, Kyoto, Japan*
[6]*Department of Developmental Biology, Graduate School of Medicine, Kyoto University, Kyoto 606-8501, Japan*
[7]*INFN, Sezione di Torino, Turin 10125, Italy*
[8]*Department of Physics and Astronomy, Heidelberg University, 69120 Heidelberg, Germany*

Cellular Potts models are broadly applied across developmental biology and cancer research. We overcome limitations of the traditional approach, which reinterprets a modified Metropolis sampling as *ad hoc* dynamics, by introducing a physical timescale through Poissonian kinetics and by applying principles of stochastic thermodynamics to separate thermal and relaxation effects from athermal noise and nonconservative forces. Our method accurately describes cell-sorting dynamics in mouse-embryo development and identifies the distinct contributions of nonequilibrium processes, e.g., cell growth and active fluctuations.

The dynamics of many nonequilibrium systems can be described by a time-dependent phenomenological Hamiltonian which actively controls transitions through a sequence of target states. Widely adopted frameworks of vertex, cellular Potts, and other methods rely on this effective energy-based principle to explain spatial organization in living systems [1–11].

Whereas the optimum of the system's energy specifies a target state of such an active transformation, the unfolding of the modeled process in time is determined by its kinetic parameters. In vertex or subcellular-element models with a continuous phase space, these parameters correspond to the transport properties—the damping coefficients. However, the traditional cellular Potts models (CPMs), whose discrete-state dynamics are implemented by a modified Metropolis sampling, lack an explicit control over such kinetic parameters.

Transport properties and the timescales they control are especially important when multiple processes evolve interdependently. In the course of embryonic development, numerous cellular and tissue-level processes require precise mutual coordination [12]. For example, the sorting of cell types in the early mouse embryo must be completed before the subsequent morphogenetic events commence [13,14].

To introduce kinetic parameters into CPMs we invoke the theory of stochastic thermodynamics [15,16], which comprehensively describes discrete-state physical processes driven by changes of free energy. As shown further, the transport properties control the system's *frenetic activity* [17], which constitutes the time-symmetric component of a *stochastic action*—the complement of entropic changes of a system's trajectory.

While being less demanding than the subcellular-element method, CPMs can treat composite materials and describe more intricate shapes than vertex models [4,18–21]. Each cell in three dimensions corresponds to a contiguous collection of voxels with the same "spin" value—labels distinguishing individual objects in the system [Fig. 1(a)].

CPMs were first introduced by Graner and Glazier [4] to study how differences of surface energy between homotypic and heterotypic contacts cause cell sorting in development. Using the modified Metropolis algorithm they found that clusters of cells emerge in a typical configuration favored by the system's energy function

$$E = \sum_{ij} \frac{J_{ij}(\sigma_i, \sigma_j)}{2} + \sum_k \frac{\kappa_k(V_k - \bar{V}_k)^2}{2}, \quad (1)$$

in which the first sum runs over spin pairs σ_i and σ_j with symmetric coefficients $J_{ij}(\sigma_i, \sigma_j) = J_{ji}(\sigma_i, \sigma_j)$ encoding the surface interactions, whereas the second term penalizes deviations of the volume V_k of the kth cell from its preferred value $\bar{V}_k$. Usually $J_{ij}(\sigma_i, \sigma_j)$ are identically zero
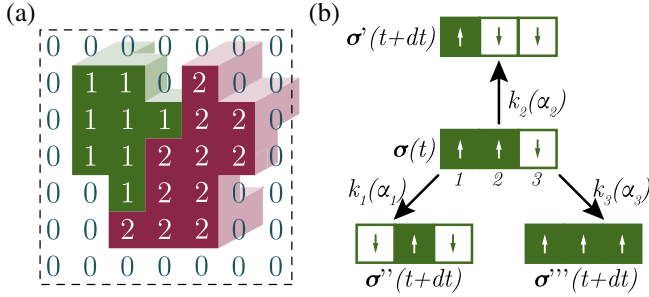
FIG. 1. (a) Schematic of a CPM: simply connected regions of a voxel grid with "spin" values 1 (green) and 2 (red) represent two cells in a medium with value 0. (b) Poissonian dynamics of three Ising spins $\boldsymbol{\sigma} = (\sigma_1, \sigma_2, \sigma_3)$: the system's configuration $\boldsymbol{\sigma}(t)$ may change within a small time dt into one of the target states ($\boldsymbol{\sigma}'$, $\boldsymbol{\sigma}''$, $\boldsymbol{\sigma}'''$), which differ from the original one by the value of a single spin $\sigma_{i=1,2,3}$, because Poissonian events never occur simultaneously.

unless the spins σ_i and σ_j are in direct contact. As the method of Graner and Glazier [4] evolved beyond a mere proof of concept, it was further generalized to include nonequilibrium aspects, such as cell division and active motility [4,11,18–38].

The modified Metropolis algorithm of modern CPMs is not the most general kinetic model for discrete systems [39–43] and has limitations [29,44]. In fact, the Metropolis scheme was originally designed to bypass slow simulations of systems' dynamics when sampling equilibrium ensembles ([45,46], Chap. 7). Since the early days of CPMs, questions have therefore been raised regarding the interpretation of time, temperature, dissipation effects, and nonequilibrium aspects of this approach [44].

As discrete-state Markovian systems, which describe continuous-time physical phenomena, CPMs can be most naturally regarded as Poissonian processes ([47], Sec. 1). The framework proposed here leverages this result of queuing theory [59] to address the above questions. Through Poissonian kinetics and stochastic thermodynamics we introduce interpretable time and energy scales, account for response coefficients and forces not incorporated in the Hamiltonian, and finally separate thermal and athermal fluctuations.

Framework.—As an illustration of our approach we first consider a paradigmatic example of discrete systems and a special case of the Potts model [60]—an Ising chain $\boldsymbol{\sigma} = (\sigma_1, \sigma_2, \ldots, \sigma_N)$ with nearest-neighbor interactions. Arranged on a one-dimensional lattice, N spins $\sigma_{i=1,2,\ldots,N} \in \{-1, 1\}$ with a periodic boundary condition $\sigma_{N+1} = \sigma_1$ are described by the Hamiltonian

$$H = \sum_{i=1}^{N} \frac{J}{2} \sigma_i \sigma_{i+1}$$

with an interaction constant J.

To define dynamics of the Ising chain we assume that each spin flips its sign with a Poissonian transition rate $k_i(\boldsymbol{\sigma})$, which in general depends on the current state $\boldsymbol{\sigma}$ [Fig. 1(b)]. Within a sufficiently small time dt at most one spin can change its value. In equilibrium, the detailed-balance condition for such a spin σ_i requires

$$\exp\left[-\frac{H(\sigma_i)}{k_B T}\right] k_i(\sigma_i) = \exp\left[-\frac{H(-\sigma_i)}{k_B T}\right] k_i(-\sigma_i), \quad (2)$$

in which $H(\sigma_i)$ and $k_i(\sigma_i)$ are, respectively, the spin's energy and transition rate, given the values of $\sigma_{j \neq i}$. From Eq. (2) it follows then

$$\frac{k_i(\sigma_i)}{k_i(-\sigma_i)} = \exp\left[-\frac{\Delta H(-\sigma_i)}{k_B T}\right], \quad (3)$$

with $\Delta H(-\sigma_i) = H(-\sigma_i) - H(\sigma_i)$.

The chain's stochastic kinetics is then given by a master equation, once a common factor between $k_i(\sigma_i)$ and $k_i(-\sigma_i)$ in Eq. (3) is specified [39,61–63]. In a general context each spin may be characterized by a state-dependent *action rate* $\alpha_i(\sigma_i)$, which determines the probability

$$1 - e^{-\alpha_i(\sigma_i)dt} \approx \alpha_i(\sigma_i)dt$$

for the ith spin to *attempt* a sign change. When such an attempt occurs, the transition probability $p(\sigma_i \to \sigma_i')$ is determined by a *directing function* $L(\sigma_i')$ with a normalization constant Z [64]

$$p(\sigma_i \to \sigma_i') = \frac{e^{L(\sigma_i')}}{Z}. \quad (4)$$

For the two possible outcomes—no change, $\sigma_i' = \sigma_i$, and a transition, $\sigma_i' = -\sigma_i$—the normalization constant expands to $Z = e^{L(\sigma_i)} + e^{L(-\sigma_i)}$ and Eq. (4) yields

$$p(\sigma_i \to \sigma_i) = \frac{1}{1 + e^{\Delta L(-\sigma_i)}}, \quad (5)$$

$$p(\sigma_i \to -\sigma_i) = \frac{e^{\Delta L(-\sigma_i)}}{1 + e^{\Delta L(-\sigma_i)}}, \quad (6)$$

with $\Delta L(-\sigma_i) = L(-\sigma_i) - L(\sigma_i)$. With the transition rate given by the product of the attempt rate and the transition probability

$$k_i(\sigma_i) = \alpha_i(\sigma_i) \frac{e^{\Delta L(-\sigma_i)}}{1 + e^{\Delta L(-\sigma_i)}}, \quad (7)$$
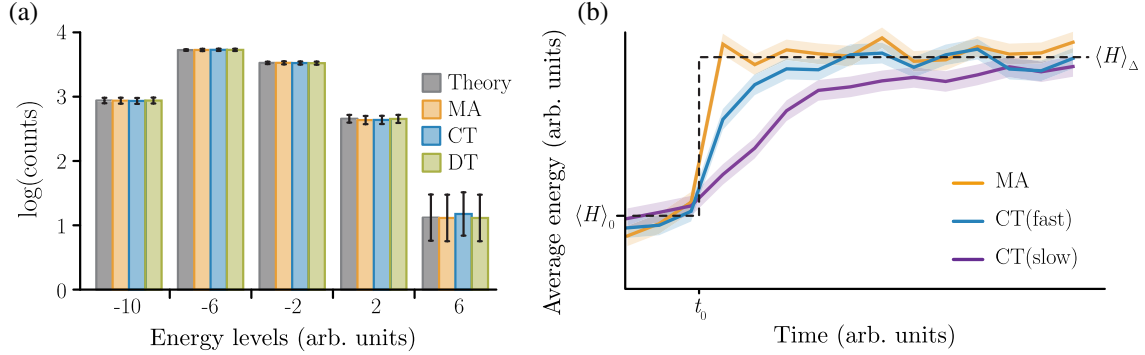
we find from Eq. (3)

FIG. 2. Simulations of an Ising chain with $N = 10$ spins. (a) Distribution of the total energy in the canonical ensemble at $T = 2J/k_B$ ($J = 1$ arb. units). Tau-leap simulations in discrete time (DT, $dt = 10^{-4}$ arb. units) match the exact distribution (theory); p value of the multinomial test 0.997 [66,67]. The continuous-time simulations (CT) and the Metropolis algorithm (MA) produce comparable results (p values 0.966 and 0.986, respectively). In the DT and CT models the chain is inhomogeneous with action rates ($\alpha_{2i+1} = 0.1$ for the odd indices, $\alpha_{2i} = 0.3$ arb. units for the even). Error bars are given by three standard deviations of 10^4 realizations. (b) Relaxation of the chain energy between two equilibrium states with average values $\langle H \rangle_0$ and $\langle H \rangle_\Delta$ at temperatures $T(t < t_0) = T_0 = 1.8|J|$ and $T(t \gg t_0) = T_0 + \Delta T = 2.0|J|/k_B$, respectively ($J = -1$ arb. units). The results of MA sampling are reported alongside the CT simulations of a slow ($\alpha_{2i} = 0.05$ and $\alpha_{2i+1} = 0.08$ arb. units) and fast ($\alpha_{2i} = 0.5$ and $\alpha_{2i+1} = 0.7$ arb. units) kinetics. Each curve traces an average over 10^4 trajectories with a standard-error band.

$$e^{\Delta L(-\sigma_i)} = \frac{\alpha_i(-\sigma_i)}{\alpha_i(\sigma_i)} \exp\left[-\frac{\Delta H(-\sigma_i)}{k_B T}\right]. \quad (8)$$

A complete specification of the Ising chain now requires both the Hamiltonian and the spins' action rates. Such a system can be simulated exactly in continuous time by the standard techniques for master equations, or approximately by using a tau-leap algorithm with a step dt [65].

The action rates do not compromise the canonical distribution of the Ising chain in equilibrium [Fig. 2(a)]. These parameters control the unfolding of dynamical processes, such as relaxation of transients. For example, chains with larger action rates, initially prepared in equilibrium at temperature T_0 and subject to a sudden temperature change ΔT, relax to the new steady state faster [Fig. 2(b)]. By design, the Metropolis scheme renders samples of the target equilibrium ensemble after a very short transient trajectory, which cannot be controlled by algorithmic or system parameters.

Model analysis.—To analyze the Poissonian dynamics of the Ising chain we apply the theory of stochastic thermodynamics. Any given trajectory of the system θ from an initial state σ^0 to a final state σ^M can be decomposed into a sequence of M elementary paths

$$\theta = \mathcal{T}_M \mathcal{T}_{M-1} \dots \mathcal{T}_1.$$

Each path $\mathcal{T}$ consists of n quiescent intervals of arbitrarily small time dt in the same configuration σ, followed by a sign change of the ith spin which produces the next state σ'. The probability of this change is $p_i \simeq k_i(\sigma_i)dt$, whereas the probability of the quiescent period lasting n steps is

$$q_n = \left[1 - dt\sum_j k_j(\sigma)\right]^n \approx e^{-n dt \sum_j k_j(\sigma)}. \quad (9)$$

With these definitions, the probability of the elementary path from a given initial condition is

$$p(\mathcal{T}|\sigma) = q_n p_i. \quad (10)$$

Now we can decompose the stochastic action $\mathcal{A}$ of the elementary path into the entropic and frenetic components [17] $\Delta\mathcal{S}$ and $\mathcal{D}$, respectively:

$$\mathcal{A} = -k_B \ln p(\mathcal{T}|\sigma) = \mathcal{D} - \frac{1}{2}\Delta\mathcal{S}. \quad (11)$$

Indeed, the probability of a time-reverse trajectory $\tilde{\mathcal{T}}$—a change of the ith spin conditioned on the initial configuration σ' and followed by n quiescent steps—is

$$p(\tilde{\mathcal{T}}|\sigma') = p_i' q_n, \quad (12)$$

in which $p_i' \approx k_i(-\sigma_i)dt$. Because of Eqs. (7) and (8) the time-asymmetric part of the action yields

$$\Delta\mathcal{S} = -k_B \ln \frac{p(\mathcal{T}|\sigma)}{p(\tilde{\mathcal{T}}|\sigma')}$$

$$= -k_B \ln \frac{k_i(\sigma_i)}{k_i(-\sigma_i)} = \frac{\Delta H(-\sigma_i)}{T}. \quad (13)$$

The time-symmetric part renders a more involved expression approximated by

$$\mathcal{D} = \frac{k_B}{2} \ln \left[p(\mathcal{T}|\boldsymbol{\sigma}) p(\tilde{\mathcal{T}}|\boldsymbol{\sigma}') \right] \approx -ndt k_B \sum_j k_j(\sigma_i)$$

$$+ k_B \ln[\sqrt{k_i(\sigma_i)k_i(-\sigma_i)}dt] \qquad (14)$$

for small dt. The total action of the whole trajectory is $\mathcal{A}(\theta) = \sum_{m=0}^{M} \mathcal{A}(\mathcal{T}_m)$ with the components

$$\Delta \mathcal{S}(\theta) = \frac{1}{T} \{ H[\boldsymbol{\sigma}^M] - H(\boldsymbol{\sigma}^0) \}, \qquad (15)$$

$$\mathcal{D}(\theta) = \sum_{m=1}^{M} \mathcal{D}(\mathcal{T}_m). \qquad (16)$$

Without compromising the entropic activity, action rates control the system's frenesy through transition rates k_j, cf. Eqs (7), (14), and (16). The entropy change of a relaxation process is entirely determined by the energy difference between the initial and final configurations of the system [Eq. (13), Fig. 2(b)]. In contrast, the frenesy depends on the kinetics of each state transition in a system's trajectory.

Poissonian cellular Potts models.—We now construct a three-dimensional Poissonian CPM [68]. Voxels on a cubic lattice describe the state of K distinct cells and a medium, taking values $\sigma_i \in \{0, 1, 2, ..., K\}$ (Fig. 1). The coefficients $J_{ij}(\sigma_i, \sigma_j)$ in Eq. (1) vanish when voxels i and j are both occupied by the same object, or when the voxel i is not within the Moore neighborhood of the voxel j [29]. Otherwise, J_{ij} assume constant positive values encoding the surface interactions between objects.

For each of the total ν object *types*, our framework introduces a Poissonian state-dependent action rate $\alpha(\sigma_i) \in \{\alpha_0, \alpha_1, ..., \alpha_\nu\}$, with which an ith voxel attempts to change its current value σ_i. Its possible target values $\sigma_i^{(j)}$ are chosen from the Von Neumann neighborhood like in the standard CPMs [29], with the transition probabilities given by a general version of Eqs. (4) and (8)

$$p(\sigma_i \to \sigma_i^{(j)}) = \frac{e^{\Delta L(\sigma_i^{(j)})}}{\sum_j e^{\Delta L(\sigma_i^{(j)})}}, \qquad (17)$$

$$e^{\Delta L(\sigma_i^{(j)})} = \frac{\alpha(\sigma_i^{(j)})}{\alpha(\sigma_i)} \exp\left[-\frac{H(\sigma_i^{(j)}) - H(\sigma_i)}{k_B T} \right]. \qquad (18)$$

Temperature in traditional CPMs is a fictitious parameter manipulated to adjust the level of fluctuations [69]. In contrast, our approach regards it as a physical variable that is set at an experimentally controlled value. To prevent cell fragmentation, usually suppressed by a periodically applied annealing, we adopt the local-connectivity test of Durand and Guesnet [29] in a modified form ([47], Sec. 3).

An extension of the directing-function formalism ([64], Appendix B) can also incorporate more general

nonequilibrium forces into Eq. (17) as

$$p(\sigma_i \to \sigma_i^{(j)}) = \frac{e^{\Delta L(\sigma_i^{(j)}) + \phi(\sigma_i, \sigma_i^{(j)})}}{\sum_j e^{\Delta L(\sigma_i^{(j)}) + \phi(\sigma_i, \sigma_i^{(j)})}}, \qquad (19)$$

in which the *active exponents* $\phi(\sigma_i, \sigma_i^{(j)})$ are functions associated with a specific transition $\sigma_i \to \sigma_i^{(j)}$, and in general $\phi(\sigma_i, \sigma_i^{(j)}) \neq \phi(\sigma_i^{(j)}, \sigma_i)$. When this perturbation breaks the detailed-balance condition, such a transition incurs an irreversible thermodynamic work.

Active exponents can introduce non-Hamiltonian forces and, by violating the fluctuation-dissipation theorem, athermal noise ([47], Sec. 2). Here, we focus on noise amplification by nonequilibrium processes, which are usually present inside cells, such as the chemically driven polymerization of cytoskeletal filaments or molecular motor activity [70–72]. If we set

$$\phi(\sigma_i, \sigma_i) \equiv 0, \qquad \phi(\sigma_i, \sigma_i^{(j)} \neq \sigma_i) = \bar{\phi} = \text{const}, \quad (20)$$

all transitions $\sigma_i \to \sigma_i^{(j)}$, except for the trivial ones $\sigma_i^{(j)} \equiv \sigma_i$ are promoted. Nonconservative forces are not generated by active exponents, whose asymmetric components vanish $\phi(\sigma_i, \sigma_i^{(j)}) - \phi(\sigma_i^{(j)}, \sigma_i) = 0$.

Specific active processes can be modeled more explicitly as well. Cell growth is typically implemented by a time-dependent preferred volume $\bar{V}_k$ in Eq. (1). Persistent cell motility can be incorporated by additional terms of the Hamiltonian [30,32–34,73], or by asymmetric active exponents.

Cell sorting during embryonic development.—As a biophysical example, we consider the sorting of epiblast (EPI) and primitive endoderm (PrE) cells in the early mouse embryo. These cells form the inner cell mass (ICM) aggregate and sort into an outer single layer of PrE cells separating the epiblast from the medium [Ref. [74], Fig. 3(a)].

Recent advances provide unprecedented experimental access to the dynamics of isolated ICMs [75–79]. We quantify the segregation of the two cell types by a *sorting score* computed from distances of EPI and PrE cells (r_i^{EPI} and r_j^{PrE}, respectively) from their common geometric center:

$$s = \frac{1}{N^{PrE} N^{EPI}} \sum_{i=1}^{N^{EPI}} \sum_{j=1}^{N^{PrE}} \text{sign}(r_j^{PrE} - r_i^{EPI}),$$

in which N^{PrE} and N^{EPI} are the numbers of PrE and EPI cells. By definition the score $s \in [-1, 1]$ is close to zero for unsorted cells, and -1 or 1 when all PrE cells are inside or outside the aggregate, respectively. To model the sorting process, we chose the five interaction constants $J_{medium:EPI}$,
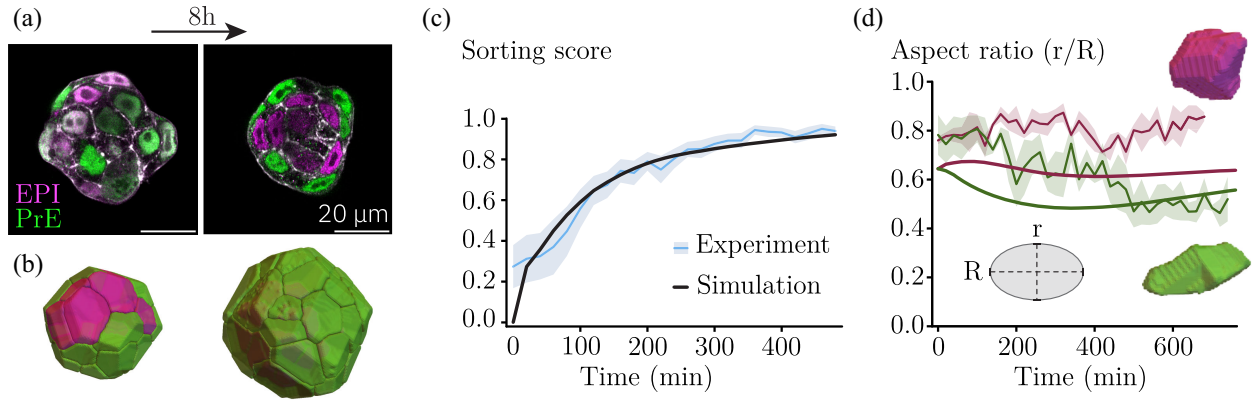
FIG. 3. Sorting of epiblast (EPI) and primitive endoderm (PrE) cells in ICMs isolated from mouse blastocysts. (a) Immunostaining images on embryonic day 3.5 and 8 h later ([47], Sec. 4). (b) Cellular-Potts simulation in the initial configuration and 8 h later. (c) Sorting score of live-imaging data averaged over eight experiments compared to a mean trend of 500 simulations [$\alpha_{0,\text{EPI,PRE}} = (0.95, 0.69, 2.12)$ min^{-1}]; standard-error band shown only for the experiments. (d) Average cellular aspect ratios characterized in the maximum-projection planes of experimental data and by the eigenvalues of the 3D gyration tensors in the simulations.

$J_{\text{medium:PrE}}$, $J_{\text{EPI:EPI}}$, $J_{\text{EPI:PrE}}$, $J_{\text{PrE:PrE}}$ from a physiologically relevant range of the EPI and PrE surface tensions, set the temperature to the experimental value at 310.15 K, and calibrated the growth parameters to match the observed proliferation dynamics ([47], Sec. 3).

Almost perfect sorting is achieved within 480 min of CPM simulations for a wide range of parameters [Fig. 3(b)]. The action rates control the relaxation dynamics of the sorting process, cf. Fig. 3(c) and Supplemental Material, Fig. S1(b) [47]. We sampled 100 combinations of the values $\{\alpha_0, \alpha_{\text{EPI}}, \alpha_{\text{PrE}}\}$, with each entry chosen from the interval $(0.10, 3.57)$ min^{-1}. The best match is closest to the experimental curve in the least-squares sense.

Furthermore, our simulations predict distinct shape dynamics of the two cell types, which quantitatively agree with the experimental data in a parameter-free comparison of cellular aspect ratios [Fig. 3(d)]: EPI cells tend to more rounded shapes, whereas PrE cells stretch normally to the radial direction at the outermost shell of ICM. For more details on ICM sorting *in vivo*, see Ref. [79].

Faster kinetics of PrE cells promote sorting [Fig. 4(a)]. This effect of inhomogeneous action rates can neither be modeled in the traditional CPMs ([47], Sec. 1), nor can it be compensated by time rescaling, as the curves parametrized by $\alpha_{0,\text{EPI,PrE}}$ in general belong to different families [Fig. 4(a)].
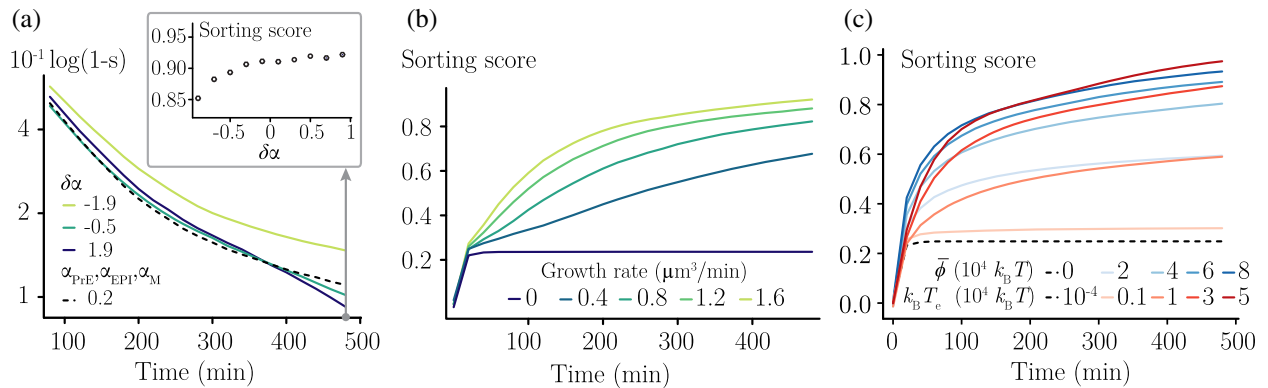

FIG. 4. Kinetic and nonequilibrium aspects of Poissonian CPMs. (a) Convergence of sorting $\log(1-s)$ for different values of heterogeneity $\delta\alpha = (\alpha_{\text{PrE}} - \alpha_{\text{Epi}})/\alpha_0$, $\alpha_0 = 1$ min^{-1}]. Inset: scores at $t = 480$ min show that faster PrE kinetics promotes sorting. Heterogeneous kinetic properties produce nonrescalable differences in the sorting dynamics—note the two-point intersection between the black dashed curve with homogeneous action rates ($\alpha_0 = \alpha_{\text{EPI}} = \alpha_{\text{PrE}} = 0.2$ min^{-1}) and the green curve ($\delta\alpha = -0.5$ min^{-1}). (b),(c) Either cell growth and division, or active fluctuations ($\bar{\phi}$), or extreme values of an *effective temperature* $k_B T_e$ are required for complete sorting. Curves in panels (a), and (b)–(c) represent averages over 1000 and 500 trajectories, respectively [parameters set to values as in Fig. 3(c) unless noted otherwise].

Without cell growth and division [Fig. 4(b)], or active fluctuations [Fig. 4(c)], sorting is hindered. Both mechanisms do a thermodynamic work on the system: the growth of cells generates stresses, and new cell boundaries increase the total surface energy, whereas the active fluctuations inject energy by breaking detailed balance. Responding to these nonequilibrium processes, the system rapidly acquires the energetically favored sorted state. Modeling active fluctuations by an effective temperature is also viable [80,81], but may misrepresent the system's response to thermodynamic forces ([47], Sec. 2).

In fact, the response coefficients of cells' surfaces are directly related to action rates ([47], Sec. 2). Because energy is a derived unit of time, "independent" rescaling of time or temperature, afforded by the traditional CPMs at the account of fictitious energy scales, is forbidden once the experimental data fix $k_B T$ and J_{ij}.

Conclusions.—Poissonian CPMs provide a physically consistent framework to study complex materials with active properties, which is generally applicable to other discrete-state systems [61–63,82]. Its kinetic parameters control transport coefficients and permit an unambiguous interpretation of time. Active fluctuations and nonequilibrium processes are clearly separated from thermal effects and passive relaxation. We applied this framework to examine the roles of distinct nonequilibrium processes in embryonic cell sorting, and show that either growth and division, or active shape fluctuations are required for successful segregation of cell types.

*roman.belousov@embl.de
†erzberge@embl.de

[1] S. Tanaka, Computation **3**, 197 (2015).
[2] A. G. Fletcher, F. Cooper, and R. E. Baker, Phil. Trans. R. Soc. B **372**, 20150519 (2017).
[3] S. Alt, P. Ganguly, and G. Salbreux, Phil. Trans. R. Soc. B **372**, 20150520 (2017).
[4] F. Graner and J. A. Glazier, Phys. Rev. Lett. **69**, 2013 (1992).
[5] J. A. Glazier and F. Graner, Phys. Rev. E **47**, 2128 (1993).
[6] T. J. Newman, Math. Biosci. Eng. **2**, 613 (2005).
[7] S. Christley, B. Lee, X. Dai, and Q. Nie, BMC Syst. Biol. **4**, 107 (2010).
[8] A. G. Fletcher, J. M. Osborne, P. K. Maini, and D. J. Gavaghan, Prog. Biophys. Molec. Biol. **113**, 299 (2013).
[9] S. Okuda, Y. Inoue, and T. Adachi, Biophys. Physicobiol. **12**, 13 (2015).
[10] C. Revell, R. Blumenfeld, and K. J. Chalut, Proc. R. Soc. B **286**, 20182495 (2019).
[11] M. Durand, PLoS Comput. Biol. **17**, e1008576 (2021).
[12] J. Negrete and A. C. Oates, Nat. Rev. Genet. **22**, 518 (2021).
[13] Y. Kojima, O. H. Tam, and P. P. Tam, Semin. Cell Dev. Biol. **34**, 65 (2014).
[14] V. Bondarenko, M. Nikolaev, D. Kromm, R. Belousov, A. Wolny, S. Rezakhani, J. Hugger, V. Uhlmann, L. Hufnagel, A. Kreshuk et al., EMBO J **42**, e113280 (2023).
[15] C. Van den Broeck, *Proceedings of the International School of Physics "Enrico Fermi"* (2013), 184, 155, ISSN 0074-784X, 10.3254/978-1-61499-278-3-155.
[16] L. Peliti and S. Pigolotti, *Stochastic Thermodynamics: An Introduction* (Princeton University Press, Princeton, NJ, 2021), ISBN 978-0-691-20177-1.
[17] C. Maes, Phys. Rep. **850**, 1 (2020).
[18] N. J. Savill and P. Hogeweg, J. Theor. Biol. **184**, 229 (1997).
[19] M. Scianna and L. Preziosi, Multiscale Model. Simul. **10**, 342 (2012).
[20] A. Voss-Böhme, PLoS One **7**, e42852 (2012).
[21] T. Hirashima, E. G. Rens, and R. M. H. Merks, Dev. Growth Diff. **59**, 329 (2017).
[22] N. Chen, J. A. Glazier, J. A. Izaguirre, and M. S. Alber, Comput. Phys. Commun. **176**, 670 (2007).
[23] V. Andasari, R. T. Roper, M. H. Swat, and M. A. J. Chaplain, PLoS One **7**, e33726 (2012).
[24] M. Scianna, L. Preziosi, and K. Wolf, Math. Biosci. Eng. **10**, 235 (2013).
[25] A. Szabó and R. M. H. Merks, Front. Oncol. **3**, 87 (2013).
[26] B. Cerruti, A. Puliafito, A. M. Shewan, W. Yu, A. N. Combes, M. H. Little, F. Chianale, L. Primo, G. Serini, K. E. Mostov et al., J. Cell Biol. **203**, 359 (2013).
[27] J. M. Osborne, Cancer Inf. **14**, 83 (2015).
[28] J. M. Belmonte, S. G. Clendenon, G. M. Oliveira, M. H. Swat, E. V. Greene, S. Jeyaraman, J. A. Glazier, and R. L. Bacallao, Mol. Biol. Cell **27**, 3673 (2016).
[29] M. Durand and E. Guesnet, Comput. Phys. Commun. **208**, 54 (2016).
[30] F. Thüroff, A. Goychuk, M. Reiter, and E. Frey, eLife **8**, e46842 (2019).
[31] M. Berghoff, J. Rosenbauer, F. Hoffmann, and A. Schug, BMC Bioinf. **21**, 436 (2020).

[32] A. J. Kabla, J. R. Soc. Interface **9,** 3268 (2012).

[33] N. Guisoni, K. I. Mazzitello, and L. Diambra, Front. Phys. **6** (2018).

[34] C. P. Beatrici, C. A. Kirch, S. Henkes, L. G. Brunnet, and F. Graner, arXiv:2210.11524.

[35] A. Nakajima and S. Ishihara, New J. Phys. **13,** 033035 (2011).

[36] A. F. M. Marée, V. A. Grieneisen, and P. Hogeweg, *The Cellular Potts Model and Biophysical Properties of Cells, Tissues and Morphogenesis* (Birkhäuser Basel, 2007), pp. 107–136, ISBN 9783764381011, 10.1007/978-3-7643-8123-3_5.

[37] R. Magno, V. A. Grieneisen, and A. F. Marée, BMC Biophys. **8** (2015).

[38] E. G. Rens and L. Edelstein-Keshet, PLoS Comput. Biol. **15,** e1007459 (2019).

[39] R. J. Glauber, J. Math. Phys. (N.Y.) **4,** 294 (1963).

[40] A. Bortz, M. Kalos, and J. Lebowitz, J. Comput. Phys. **17,** 10 (1975).

[41] A. Prados, J. J. Brey, and B. Sánchez-Rey, J. Stat. Phys. **89,** 709 (1997).

[42] S. A. Serebrinsky, Phys. Rev. E **83,** 037701 (2011).

[43] M. Zeegers, Bachelor's thesis, Leiden Institute of Advanced Computer Science (LIACS), Leiden University, Niels Bohrweg 1, 2333 CA Leiden, The Netherlands (2013), https://liacs.leidenuniv.nl/assets/Bachelorscripties/2012-2013-17MatheZeegers.pdf.

[44] J. A. Glazier, A. Balter, and N. J. Popławski, *Magnetization to Morphogenesis: A Brief History of the Glazier-Graner-Hogeweg Model* (Birkhäuser Basel, 2007), pp. 79–106, ISBN 9783764381011, 10.1007/978-3-7643-8123-3_4.

[45] N. Metropolis, A. W. Rosenbluth, M. N. Rosenbluth, A. H. Teller, and E. Teller, J. Chem. Phys. **21,** 1087 (1953),

[46] M. Tuckerman, *Statistical Mechanics: Theory and Molecular Simulation* (OUP, Oxford, 2010), ISBN 978-0-19-152346-5.

[47] See Supplemental Material at http://link.aps.org/supplemental/10.1103/PhysRevLett.132.248401 for further theoretical, computational, and experimental details, which include also Refs. [48–58].

[48] E. Bringuier, Eur. J. Phys. **32,** 975 (2011).

[49] D. Andreucci, E. N. M. Cirillo, M. Colangeli, and D. Gabrielli, J. Stat. Phys. **174,** 469 (2018).

[50] J. B. Keller, Proc. Natl. Acad. Sci. U.S.A. **101,** 1120 (2004).

[51] S. Chandrasekhar, Rev. Mod. Phys. **15,** 1 (1943).

[52] R. Belousov, E. G. D. Cohen, and L. Rondoni, Phys. Rev. E **94,** 032127 (2016).

[53] A. W. C. Lau and T. C. Lubensky, Phys. Rev. E **76,** 011123 (2007).

[54] F. Graner and D. Riveline, Development **144,** 4226 (2017).

[55] J. Kopp, Int. J. Mod. Phys. C **19,** 523 (2008).

[56] M. J. Kronenburg, arXiv:1306.6291.

[57] C.-A. Deledalle, L. Denis, S. Tabti, and F. Tupin, Closed-form expressions of the eigen decomposition of 2×2

and 3×3 Hermitian matrices (2017), https://hal.science/hal-01501221.

[58] J.-L. Maître, R. Niwayama, H. Turlier, F. Nédélec, and T. Hiiragi, Nat. Cell Biol. **17,** 849 (2015).

[59] R. B. Nelsen, Am. Math. Mon. **94,** 981 (1987).

[60] F. Y. Wu, Rev. Mod. Phys. **54,** 235 (1982).

[61] T. Herpich, J. Thingna, and M. Esposito, Phys. Rev. X **8,** 031056 (2018).

[62] N. Freitas, J.-C. Delvenne, and M. Esposito, Phys. Rev. X **11,** 031064 (2021).

[63] J. Meibohm and M. Esposito, Phys. Rev. Lett. **128,** 110603 (2022).

[64] R. Belousov, A. Hassanali, and É. Roldán, Phys. Rev. E **106,** 014103 (2022).

[65] D. T. Gillespie, J. Chem. Phys. **115,** 1716 (2001).

[66] D. N. Lawley, Biometrika **43,** 295 (1956).

[67] D. A. Williams, Biometrika **63,** 33 (1976).

[68] Source code, which implements the Poissonian cellular Potts model described in this letter, is available online https://git.embl.de/rbelouso/dycpm/.

[69] M. H. Swat, G. L. Thomas, J. M. Belmonte, A. Shirinifard, D. Hmeljak, and J. A. Glazier, in *Methods in Cell Biology* (Elsevier, New York, 2012), pp. 325–366, 10.1016/B978-0-12-388403-9.00013-8.

[70] K. Kruse, J. F. Joanny, F. Jülicher, J. Prost, and K. Sekimoto, Eur. Phys. J. E **16,** 5 (2005).

[71] F. Julicher, K. Kruse, J. Prost, and J. Joanny, Phys. Rep. **449,** 3 (2007).

[72] V. Laplaud, N. Levernier, J. Pineau, M. S. Roman, L. Barbier, P. J. Sáez, A.-M. Lennon-Duménil, P. Vargas, K. Kruse, O. du Roure *et al.*, Sci. Adv. **7,** eabe3640 (2021).

[73] J. M. Belmonte, G. L. Thomas, L. G. Brunnet, R. M. C. de Almeida, and H. Chaté, Phys. Rev. Lett. **100,** 248702 (2008).

[74] N. Saiz, L. Mora-Bitria, S. Rahman, H. George, J. P. Herder, J. Garcia-Ojalvo, and A.-K. Hadjantonakis, eLife **9,** e56079 (2020).

[75] D. Solter and B. B. Knowles, Proc. Natl. Acad. Sci. U.S.A. **72,** 5099 (1975).

[76] M. Wigger, K. Kisielewska, K. Filimonow, B. Plusa, M. Maleszewski, and A. Suwińska, Sci. Rep. **7,** 15136 (2017).

[77] E. J. Y. Kim, L. Sorokin, and T. Hiiragi, Development **149,** dev200140 (2022).

[78] A. Yanagida, E. Corujo-Simon, C. K. Revell, P. Sahu, G. G. Stirparo, I. M. Aspalter, A. K. Winkel, R. Peters, H. D. Belly, D. A. Cassani *et al.*, Cell **185,** 777 (2022).

[79] P. Moghe, R. Belousov, T. Ichikawa, C. Iwatani, T. Tsukiyama, F. Graner, A. Erzberger, and T. Hiiragi (2023), 10.1101/2023.05.16.540918.

[80] L. F. Cugliandolo, J. Kurchan, and L. Peliti, Phys. Rev. E **55,** 3898 (1997).

[81] M. Polettini and M. Esposito, J. Stat. Phys. **176,** 94 (2019).

[82] A. P. Solon and J. Tailleur, Phys. Rev. Lett. **111,** 078101 (2013).